Published in final edited form as:
ACS Catal. 2018 ; 8(9): . doi:10.1021/acscatal.8b02212.

Highly Dispersed Platinum on Honeycomb-like NiO@Ni Film as a Synergistic Electrocatalyst for the Hydrogen Evolution Reaction

Zheng-Jun Chen[†,§], **Guo-Xuan Cao**[†,§], **Li-Yong Gan**[*,†], **Hao Dai**[†], **Ning Xu**[†], **Ming-Jie Zang**[†], **Hong-Bin Dai**[†], **Hui Wu**[‡], **Ping Wang**[*,†]

[†]School of Materials Science and Engineering, Key Laboratory of Advanced Energy Storage Materials of Guangdong Province, South China University of Technology, Guangzhou 510641, People's Republic of China

[‡]NIST Center for Neutron Research, National Institute of Standards and Technology, Gaithersburg, Maryland 20899-6102, United States

Abstract

Platinum (Pt) is well-known as the best-performing catalyst for the hydrogen evolution reaction (HER), but its practical application is severely hindered by its prohibitively high cost and problematic performance in alkaline electrolyte. Herein, we report that the issues of intrinsic activity and cost concern of Pt can be simultaneously addressed by employing a combination of concerted catalysis and nanoengineering strategies. Motivated by our density functional theory (DFT) calculations that the cooperative catalysis between Pt and NiO would lead to a better HER activity in comparison to Pt solely in alkaline solution, we successfully synthesized a Pt/NiO@Ni/NF nanocomposite catalyst by depositing highly dispersed Pt nanoclusters/nanoparticles on a honeycomb-like NiO@Ni film supported on Ni foam (NF). The resulting Pt/NiO@Ni/NF catalyst outperforms the commercial Pt/C catalyst with a high and stable HER activity in alkaline solution and, more impressively, with an economical Pt content as low as ~0.1 mg cm^{-2}.

Graphical abstract

[*]**Corresponding Authors** L.-Y.G.: ganly@scut.edu.cn. P.W.: mspwang@scut.edu.cn.
[§]Z.-J.C. and G.-X.C. contributed equally.

■ASSOCIATED CONTENT

Supporting Information
The Supporting Information is available free of charge on the ACS Publications website at DOI: 10.1021/acscatal.8b02212.
Experimental details and supplementary characterization results (PDF)

The authors declare no competing financial interest.

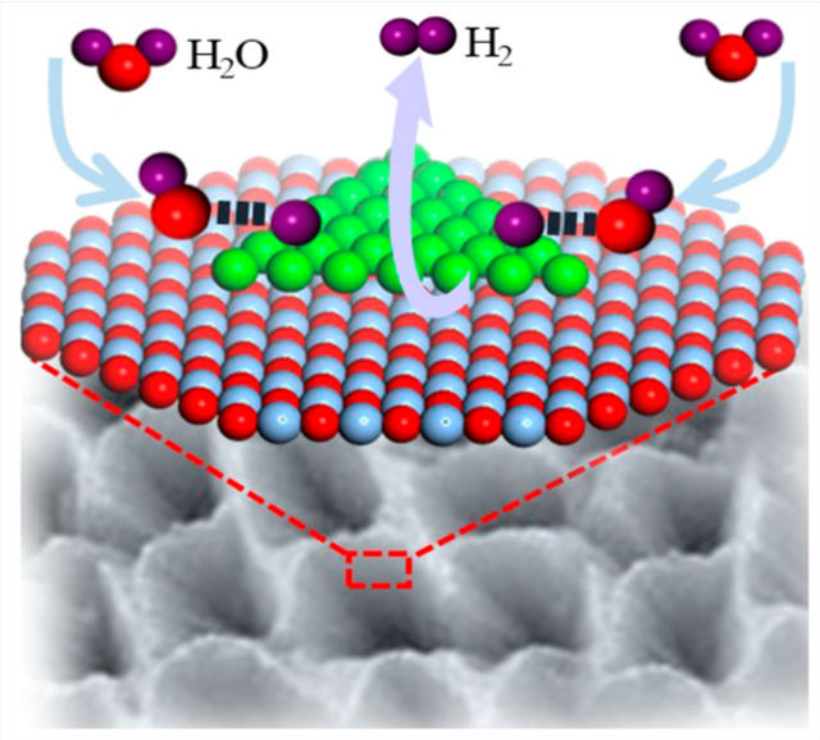

Keywords

hydrogen evolution reaction; electrocatalyst; concerted catalysis; nanoengineering strategy; intrinsic activity

1. INTRODUCTION

Hydrogen gas (H_2) is expected to play a central role in future fuel cell technology. Electrochemical water splitting provides an eco-friendly and sustainable way to produce hydrogen fuel and breathable oxygen. Crucial to enabling an energy-efficient water splitting is the development of active, durable, and cost-effective electrocatalysts for the hydrogen evolution reaction (HER) and oxygen evolution reaction (OER).[1–3]

Platinum (Pt) is well-known as a benchmark catalyst for its best performance in HER, but it is also infamous for its high cost and scarcity.[4] In past decades, extensive research activities have been directed toward the development of cost-effective alternatives to Pt. These have resulted in the identification of a variety of promising HER catalysts free of precious metals such as sulfides,[5,6] phosphides,[7,8] carbides,[9,10] nitrides,[11] selenides,[12] and borides.[13,14] Despite this encouraging progress, the use of nonprecious metals should not be the exclusive approach to developing practical electrocatalysts. Enhancing the utilization efficiency of noble metals may also provide a realistic approach to the development of high-performance and cost-effective catalysts.[15,16] This has been exemplified by recent several studies. It was found that catalysts surface-decorated by a small amount of Pt in the forms of

a single-atom, cluster, or monolayer coating exhibit catalytic performance comparable to or even better than that of Pt/C or Pt foil catalysts.[17−21]

Due to the concern that most nonprecious OER catalysts are vulnerable in strongly acidic media, electrolysis of water in alkaline media appears to be more realistic for practical H_2 production.[22,23] However, for the benchmark Pt catalyst, its catalytic performance under alkaline conditions is significantly inferior to that under acidic conditions.[24,25] It was recently recognized that the pH-dependent catalytic performance of Pt might be associated with the variations of HER pathways.[26] The stepwise HER in alkaline solutions involves dissociation of H_2O and the succeeding associative desorption of an H_2 molecule.[27] While Pt is well-known to be a good catalyst for the latter step, the overall sluggish HER kinetics in alkaline solutions stem from the insufficient catalyzing capability of Pt toward the cleavage of the H−OH bond.[28,29] A strategy for circumventing this problem is to create concerted catalysts with a combination of metal oxides and Pt, where the oxides promote the dissociation of H_2O and the nearby Pt facilitates the adsorption and recombination of the resulting H intermediates into molecular H_2.[27,30−34] A recent work by Jin et al. developed a novel in situ reduction method to synthesize Pt nanocrystal decorated two-dimensional $Ni(OH)_2$. As a consequence of well-regulated growth of heterostructural interfaces, the Pt/$Ni(OH)_2$ nanocomposite catalyst exhibited pronounced HER activity in alkaline solution.[35]

In the present study, we employed a combination of concerted catalysis and nanoengineering strategies to simultaneously address the issues of intrinsic activity and utilization efficiency of Pt. Our density functional theory (DFT) calculations illustrated that the cooperation between Pt and nickel oxide (NiO) would lead to a more pronounced catalytic activity toward the HER than Pt alone. Experimentally, we first synthesized a nanoporous nickel oxide/nickel (NiO@Ni, denoting a shell−core structure) film supported on nickel foam (NF) using electrodeposition combined with selective electrochemical etching methods. Tiny Pt nanoclusters/nanoparticles were then deposited on the surface of NiO@ Ni film using a strong electrostatic adsorption (SEA) method followed by electrochemical reduction. The resulting Pt/ NiO@Ni/NF catalyst exhibits exceptionally high and stable activity toward the HER in alkaline solution, which is even superior to that of Pt/C catalyst. Notably, such outstanding catalytic performance was achieved in a catalyst with a sparing Pt content below 0.1 mg cm^{-2}.

2. RESULTS AND DISCUSSION

In the present study, we chose NiO to cooperate with Pt to provide active sites for a collective catalysis of the HER. This selection was based on the following considerations: NiO was known to be effective for promoting water dissociation.[36,37] Ni was used as the substrate in the present work, an adherent and coherent NiO passivation film will be naturally formed on the Ni surface under oxidation conditions. This ensures a favorable combination of the advantages such as simplified preparation procedures, thin thickness of the NiO layer, and a good interfacial contact between the substrate and electrocatalytic materials.

2.1. Theoretical Study of the Concerted Catalysis of HER by Pt and NiO.

DFT calculations were first conducted to evaluate the effect of the cooperation between Pt and NiO on the HER. Specifically, the elementary reaction steps involved in the alkaline HER, i.e., dissociation of an H_2O molecule and the subsequent associative desorption of an H_2 molecule, were investigated on the NiO/Pt interface and Pt surface, respectively (Figure S1 in the Supporting Information). Figure 1 shows the calculated free energy diagram for the HER on the two modeled surfaces. H_2O dissociation on Pt (111) is remarkably endothermic (0.80 eV) with a large energy barrier (1.01 eV), indicating a rather sluggish Volmer step on the Pt surface.[27,38] In sharp contrast, the dissociation barrier of H_2O at the NiO/Pt interface is significantly reduced by over 40%, highlighting the pivotal role of NiO in promoting H_2O dissociation and substantially enhancing the production of H* (* donates an adsorption site). The resulting H intermediate from H_2O dissociation can readily convert into molecular H_2 on the Pt (111) surface with a calculated ΔG(H*) value of only −0.06 eV.[39] In addition, the free energy change of *OH desorption from the NiO surface to form OH^-, $\Delta G(OH^-)$, was calculated to be 68 meV, suggesting an easy desorption.[40] These calculation results clearly suggest that NiO and Pt may work in concert to properly address different elementary steps of the HER and thereby synergistically provide highly active sites to catalyze the HER in an alkaline solution.

2.2. Synthesis and Characterization of Electrocatalysts.

We then employed a series of carefully designed procedures to synthesize and ensure simultaneously a high density of catalytically active sites and an improved utilization efficiency of Pt. Figure 2 schematically shows the preparation process of the targeted Pt/NiO@Ni/NF catalyst, which involves four sequential steps. First, a supported Ni/Cu film was deposited on NF by electrodeposition. An electrochemical etching method was then applied to selectively strip Cu from Ni/Cu film at positive potentials. The resulting NiO@Ni/NF sample was then submerged into a H_2PtCl_6 solution, in which the $[PtCl_6]^{2-}$ ions were electrostatically adsorbed onto the NiO surface via controlling the pH value of the solution below the isoelectric point of NiO. The thus-prepared sample was finally subjected to an electrochemical reduction process to obtain the targeted Pt/NiO@Ni/NF catalyst. The Pt content was measured by inductively coupled plasma−atomic emission spectrometry (ICP-AES). According to the concentration change of $[PtCl_6]^{2-}$ before and after the electrostatic adsorption process, the loading amount of Pt on the targeted catalyst was determined to be 0.092 mg cm^{-2}.

Morphological observation of the electrodeposited sample by field-emission scanning electron microscopy (FE-SEM) found that the surface of NF was entirely covered by large numbers of the nanoislands with different shapes (Figure 3a). The X-ray diffraction (XRD) pattern (Figure 4a) of the aselectrodeposited film can be well indexed to crystalline Ni (JCPDS Card 87–0712) and Cu (JCPDS Card 85–1326). After the electrochemical etching, the sample showed notable changes in the surface morphology. As seen in Figure 3b,c, the etched sample presents a honeycomb-like nanoporous structure, wherein the columnar pores ranging from 50 to 200 nm in diameter and pore walls of ~20 nm in thickness interconnected to form a network. According to the FE-SEM observation of the etched sample (Figure S2 in the Supporting Information), the thickness of the supported

nanoporous film on NF was 300−500 nm. The parallel XRD analysis of the etched sample clearly showed that the diffraction peaks of Cu completely disappeared and those of Ni remained. Evidently, it was the selective removal of Cu and surface passivation of Ni under the controlled anodic potential that resulted in the formation of the nanoporous structure. Here, the invisibility of the NiO passivation film in the XRD analysis should be due to the small amount formed during the electrochemical etching process. However, its presence on the sample surface was indeed evidenced by Raman spectra and X-ray photoelectron spectroscopy (XPS) analyses. As seen in Figure 4b, the etched sample clearly showed the characteristic bands of NiO at 1065.63 and 525.62 cm^{-1}, respectively.[41,42] The XPS Ni 2p spectra (Figure 4c) of the etched sample can be resolved fairly well into Ni^0 and Ni^{2+} doublets and satellite features. In an effort to evaluate the thickness of NiO film, we further conducted the XPS depth profile analysis of the NiO@Ni/NF sample. As seen in Figure S3 in the Supporting Information, the sample surface initially showed a dominant Ni^{2+} signal. When the sample was exposed to an Ar^+ beam, the Ni^{2+} signal gradually weakened and the Ni^0 signal intensified with an increase in the sputtering time. After etching was carried out for 100 s, the signal intensities of Ni^{2+} and Ni^0 became largely stable. On the basis of the published sputter yield data and the applied experimental parameters, the etch depth after 100 s of Ar^+ sputtering was calculated to be around 11 nm.[43] This gives a quantitative estimation of the thickness of the NiO film.

The deposition of Pt onto the surface of the NiO@Ni/NF sample was conducted by SEA followed by electrochemical reduction. The resulting catalyst sample was examined by XPS to determine the composition and chemical states of the constituent elements on the catalyst surface. As seen in Figure 4d, the Pt signal was clearly identified by XPS, and the Pt 4f spectrum could be fitted with two doublets assigned to the dominant Pt^0 and minor Pt^{2+} species, respectively. Careful examination of the coexistent Ni 3p signal in the Pt 4f region (Figure 4d) and the Ni 2p spectra (Figure 4c) further suggested that there should be no significant change in the chemical state of Ni after the deposition of Pt on the surface of the NiO@Ni/NF sample. Additionally, FE-SEM and transmission electron microscopy (TEM) observations found that the surface morphology of the NiO@Ni/NF sample was well retained after the Pt deposition (Figure 3d and Figure S4a,b in the Supporting Information). Figure 3e presents the selected area electron diffraction (SAED) pattern of the Pt/NiO@Ni/NF sample, which showed a series of concentric rings that matched well with the crystalline planes of NiO and Ni. Consistently, the lattice fringes corresponding to the (200) and (111) crystal planes of NiO and the (111) plane of Ni were clearly observed in the high-resolution TEM (HRTEM) image (Figure 3f). In addition, the HRTEM images (Figure 3f and Figure S5 in the Supporting Information) showed the thickness of the NiO film ranging from ~5 to 20 nm. This is in good agreement with the results from the XPS depth analysis. Notably, it was difficult to observe the distribution of Pt^0 species in the HRTEM image, which is indicative of its tiny size. This was further validated by the two-dimensional elemental mapping results that were acquired in high-angle annular dark-field scanning transmission electron microscopy (HAADF-STEM) mode in combination with energy dispersive X-ray spectroscopy (EDX) analysis. As seen in Figure 3g,h, the overwhelming majority of Pt atoms were uniformly dispersed on the sample surface in the form of nanoclusters or tiny nanoparticles. However, from the parallel EDX line-scanning

profile analysis, we did obtain more detailed information about the distribution state of Pt^0 species (Figure S6 in the Supporting Information). It was observed that the Pt signal became intensified in the central region of the analyzed nanoparticles, and no regular correlation between the distribution of Pt and Ni signals was observed. These results implied that the Pt element existed mainly in the form of metallic Pt with an average size of around 2 nm. In comparison, the TEM image of the Pt/C catalyst (Figure S7 in the Supporting Information) showed a broader size distribution (from several nanometers to over 10 nm) and noticeable aggregation of Pt nanoparticles. Evidently, a homogeneous dispersion of tiny Pt nanoparticles is favorable for optimizing its utilization efficiency. In the Pt/NiO@Ni/NF sample, the favorable distribution state of Pt on the catalyst surface should be ascribed to the small loading amount and the employment of the SEA method. As the interaction between metal ion complex and oxide substrate is essentially Coulombic in nature, SEA is a powerful method for producing uniformly distributed $[PtCl_6]^{2-}$ onto the NiO surface, ideally to form a monolayer.[44,45] In a control experiment to identify the effect of NiO, we prepared a Pt-deposited sample (denoted as Pt@Ni/ NF) using a galvanic replacement method. The only difference between the Pt@Ni/NF sample and the aforementioned Pt/ NiO@Ni/NF sample is that in the control sample the NiO@ Ni/NF film substrate was treated with hydrochloric acid (HCl) solution to remove the NiO passivation film before Pt deposition. As shown in Figure 3i, the STEM-EDX image showed aggravated aggregation of Pt on the Pt@Ni/NF sample surface.

2.3. Electrocatalytic HER Performance.

The HER activity of Pt/NiO@Ni/NF catalyst was evaluated in 1.0 M potassium hydroxide (KOH) solution by linear sweep voltammetry in a standard three-electrode system. For comparison, the bare NF, NiO@Ni/NF, the commercial Pt/ C (20 wt %) catalyst, and the Pt@Ni/NF sample prepared by a galvanic replacement method were measured under identical conditions. As depicted in Figure 5a, the Pt/NiO@Ni/NF electrocatalyst exhibited much higher HER activity in comparison to all the other samples, including the Pt/C catalyst. It required an overpotential of only 34 mV to reach a current density of 10 mA cm^{-2} under alkaline conditions, which is among the best reported levels for HER catalysts (Table S1 in the Supporting Information). The property advantages of Pt/NiO@Ni/NF over the other tested catalysts were further highlighted from comparisons of the mass-specific activity and the turnover frequency (TOF). It was found that the mass current density (based on the mass of Pt) of the Pt/ NiO@Ni/NF catalyst reached up to 532 A g_{Pt}^{-1} at −0.05 V, which was dramatically higher than that of the commercial Pt/ C (35 A g_{Pt}^{-1}) and Pt@Ni/NF (250 A g_{Pt}^{-1}) (Figure 5b). The calculated TOF values of the Pt/ NiO@Ni/NF catalyst at different overpotentials were also significantly greater than those of the Pt@Ni/NF and the commercial Pt/C, providing a nearly full Pt participation in the catalytic reaction (Figure S8 in the Supporting Information). The remarkably higher HER activity of Pt/NiO@Ni/NF in comparison to the Pt/C and Pt@Ni/NF catalysts in alkaline solutions might be understood from two aspects. (i) Pt and NiO work in concert to provide active sites for both H_2O dissociation and H_2 desorption steps, which possess higher intrinsic HER activity than Pt alone in alkaline solutions. This is in good agreement with our DFT calculations. (ii) Uniform dispersion of tiny Pt nanoclusters/ nanoparticles on the NiO

surface ensures an enhanced utilization efficiency of metal Pt, leading to a large number of active sites readily accessible to the reactants.

Tafel analysis of the polarization curves may provide valuable insight into the HER mechanism. As seen in Figure 5c, the Tafel slope of Pt/NiO@Ni/NF was determined to be 39 mV dec^{-1}, which is lower than those of Pt/C (52 mV dec^{-1}) and Pt@Ni/NF (56 mV dec^{-1}). According to the current mechanistic understanding, the HER over these Pt-containing electrocatalysts proceeds via a Volmer−Heyrovsky mechanism.[46] The low Tafel slope of Pt/NiO@Ni/NF catalyst is indicative of an accelerated Volmer step by a rational combination of Pt with NiO, consistent with our DFT calculations. An electrochemical impedance spectroscopy (EIS) analysis was further employed to investigate the electrode kinetics in the HER process. As shown in Figure 5d, Pt/NiO@Ni/NF, Pt@Ni/NF, and NiO@Ni/NF samples showed similar low charge transfer resistance (R_{ct}) values, all in a range of 3.51−5.48 Ω. As NiO is a poor electron conductor, these results clearly suggested that NiO should be present in a form of an ultrathin film. This was also supported by HRTEM (Figure 3f and Figure S5 in the Supporting Information) and XPS depth profile (Figure S3 in the Supporting Information) analyses. Moreover, the small R_{ct} value of the Pt/NiO@Ni/NF catalyst also implied a good interface contact between Pt and NiO. The affinity of Pt and NiO in the Pt/NiO@Ni/NF catalyst was further evidenced by our temperature-programmed reduction (TPR) measurements. As seen in the TPR profiles (Figure S9 in the Supporting Information), the reduction peak of NiO in the NiO@Ni/NF sample appeared at ~270 °C. In contrast, the Pt/NiO@Ni/NF sample showed two peaks of NiO reduction. The appearance of the low-temperature reduction peak of NiO (~220 °C) could be safely ascribed to hydrogen spillover from Pt to NiO and is thereby an indication of the close proximity between Pt and NiO. Therefore, an ultrathin film form of NiO and its excellent interface contact with Pt should be responsible for the good electric conductivity, which is desirable for fast HER kinetics and is a prerequisite for the overall HER catalyzing performance of the Pt/NiO@Ni/NF composite catalyst.

Durability is another important criterion in the evaluation of HER electrocatalysts. In the present study, we tested the durability of the Pt/NiO@Ni/NF catalyst using a chronopotentiometric method. As shown in Figure 5e, the overpotential increase of the Pt/NiO@Ni/NF catalyst after 24 h of constant-current tests was much smaller than those for the relevant Pt/ C and NiO@Ni/NF catalysts. SEM observations found that the morphological features of the Pt/NiO@Ni/NF electrocatalyst were well retained after long-term operations (Figure S4c,d in the Supporting Information). These results indicated a good stability of the Pt/NiO@Ni/NF electrocatalyst for the HER under alkaline conditions. The Faradaic efficiency (FE) of the HER was also measured at a current density of 10 mA cm^{-2}. As shown in Figure 5f, the collected amounts of H_2 at different reaction durations matched well with the theoretical values, indicating a near-unity FE.

3. CONCLUSION

In summary, our initial predictive DFT calculations envisaged that the cooperation between Pt and NiO would lead to a more pronounced catalytic activity toward the HER in comparison to solely Pt in alkaline electrolyte. We experimentally implemented this

conception by a successful synthesis of a Pt/NiO@Ni/NF nanocomposite catalyst via depositing highly dispersed Pt nanoclusters/nanoparticles on a nanoporous NiO@Ni film supported on Ni foam. Benefiting from the high utilization efficiency of Pt and the concerted catalysis between Pt and the NiO film, the Pt/NiO@Ni/NF nanocomposite catalyst with a Pt content as low as ~0.1 mg cm^{-2} exhibited high and stable activity toward the HER in alkaline solution, which is among the top reported levels for HER electrocatalysts. Our study showed that simultaneous enhancement of both the intrinsic activity and the utilization efficiency of noble metals may also provide a realistic approach for the development of high-performance and cost-effective elecctrocatalysts for energy conversion applications.

Supplementary Material

Refer to Web version on PubMed Central for supplementary material.

ACKNOWLEDGMENTS

Financial support is acknowledged from the National Natural Science Foundation of China (Grant Nos. 51671087 and 11504303), the Foundation for Innovative Research Groups of the National Natural Science Foundation of China (Grant No. 51621001), the Foundation for Research Groups of the Natural Science Foundation of Guangdong Province (Grant No. 2016A030312011), and the Special Support Plan for National 10000-talents Program.

REFERENCES

(1). Nørskov JK; Christensen CH. Toward Efficient Hydrogen Production at Surfaces. Science 2006, 312, 1322–1323. [PubMed: 16741103]

(2). Roger I; Shipman MA; Symes MD. Earth-Abundant Catalysts for Electrochemical and Photoelectrochemical Water Splitting. Nat. Rev. Chem. 2017, 1, 0003.

(3). Seh ZW; Kibsgaard J; Dickens CF; Chorkendorff IB; Nørskov JK; Jaramillo TF. Combining Theory and Experiment in Electrocatalysis: Insights into Materials Design. Science 2017, 355, eaad4998. [PubMed: 28126774]

(4). Wang X; Gan X; Hu T; Fujisawa K; Lei Y; Lin Z; Xu B; Huang ZH; Kang F; Terrones M; Lv R. Noble-Metal-Free Hybrid Membranes for Highly Efficient Hydrogen Evolution. Adv. Mater. 2017, 29, 1603617.

(5). Wu Z; Li X; Liu W; Zhong Y; Gan Q; Li X; Wang H. Materials Chemistry of Iron Phosphosulfide Nanoparticles: Synthesis, Solid State Chemistry, Surface Structure, and Electrocatalysis for the Hydrogen Evolution Reaction. ACS Catal. 2017, 7, 4026–4032.

(6). Shi Y; Zhou Y; Yang DR; Xu WX; Wang C; Wang FB; Xu JJ; Xia XH; Chen HY. Energy Level Engineering of MoS_2 by Transition-Metal Doping for Accelerating Hydrogen Evolution Reaction. J. Am. Chem. Soc. 2017, 139, 15479–15485. [PubMed: 29032672]

(7). Liu T; Liu D; Qu F; Wang D; Zhang L; Ge R; Hao S; Ma Y; Du G; Asiri AM; Chen L; Sun X. Enhanced Electrocatalysis for Energy-Efficient Hydrogen Production over CoP Catalyst with Nonelectroactive Zn as a Promoter. Adv. Energy Mater. 2017, 7, 1700020.

(8). Xiao P; Sk MA; Thia L; Ge X; Lim RJ; Wang JY; Lim KH; Wang X. Molybdenum Phosphide as an Efficient Electrocatalyst for the Hydrogen Evolution Reaction. Energy Environ. Sci. 2014, 7, 2624–2629.

(9). Li JS; Wang Y; Liu CH; Li SL; Wang YG; Dong LZ; Dai ZH; Li YF; Lan YQ. Coupled Molybdenum Carbide and Reduced Graphene Oxide Electrocatalysts for Efficient Hydrogen Evolution. Nat. Commun. 2016, 7, 11204. [PubMed: 27032372]

(10). Lu C; Tranca D; Zhang J; Hernandez FR; Su Y; Zhuang X; Zhang F; Seifert G; Feng X. Molybdenum Carbide-Embedded Nitrogen-Doped Porous Carbon Nanosheets as Electrocatalysts for Water Splitting in Alkaline Media. ACS Nano 2017, 11, 3933–3942. [PubMed: 28291319]

(11). Zhu Y; Chen G; Xu X; Yang G; Liu M; Shao Z. Enhancing Electrocatalytic Activity for Hydrogen Evolution by Strongly Coupled Molybdenum Nitride@Nitrogen-Doped Carbon Porous Nano-Octahedrons. ACS Catal. 2017, 7, 3540–3547.

(12). Xia C; Liang H; Zhu J; Schwingenschlügl U; Alshareef HN. Active Edge Sites Engineering in Nickel Cobalt Selenide Solid Solutions for Highly Efficient Hydrogen Evolution. Adv. Energy Mater. 2017, 7, 1602089.

(13). Li H; Wen P; Li Q; Dun C; Xing J; Lu C; Adhikari S; Jiang L; Carroll DL; Geyer SM. Earth-Abundant Iron Diboride (FeB2) Nanoparticles as Highly Active Bifunctional Electrocatalysts for Overall Water Splitting. Adv. Energy Mater. 2017, 7, 1700513.

(14). Zhuang Z; Li Y; Li Z; Lv F; Lang Z; Zhao K; Zhou L; Moskaleva L; Guo S; Mai L. MoB/g-C_3N_4 Interface Materials as a Schottky Catalyst to Boost Hydrogen Evolution. Angew. Chem., Int. Ed. 2018, 57, 496–500.

(15). Stephens IEL; Chorkendorff I. Minimizing the Use of Platinum in Hydrogen-Evolving Electrodes. Angew. Chem., Int. Ed. 2011, 50, 1476–1477.

(16). Jiao Y; Zheng Y; Jaroniec M; Qiao SZ. Design of Electrocatalysts for Oxygen- and Hydrogen-Involving Energy Conversion Reactions. Chem. Soc. Rev. 2015, 44, 2060–2086. [PubMed: 25672249]

(17). Li M; Ma Q; Zi W; Liu X; Zhu X; Liu S. Pt Monolayer Coating on Complex Network Substrate with High Catalytic Activity for the Hydrogen Evolution Reaction. Sci. Adv. 2015, 1, e1400268.

(18). Cheng N; Stambula S; Wang D; Banis MN; Liu J; Riese A; Xiao B; Li R; Sham TK; Liu LM; Botton GA; Sun X. Platinum Single-Atom and Cluster Catalysis of the Hydrogen Evolution Reaction. Nat. Commun. 2016, 7, 13638. [PubMed: 27901129]

(19). Chao T; Luo X; Chen W; Jiang B; Ge J; Lin Y; Wu G; Wang X; Hu Y; Zhuang Z; Wu Y; Hong X; Li Y. Atomically Dispersed Copper-Platinum Dual Sites Alloyed with Palladium Nanorings Catalyze the Hydrogen Evolution Reaction. Angew. Chem., Int. Ed. 2017, 56, 16047–16051.

(20). Zhang L; Han L; Liu H; Liu X; Luo J. Potential-Cycling Synthesis of Single Platinum Atoms for Efficient Hydrogen Evolution in Neutral Media. Angew. Chem., Int. Ed. 2017, 56, 13694–13698.

(21). Zhang H; An P; Zhou W; Guan BY; Zhang P; Dong J; Lou XW. Dynamic Traction of Lattice-Confined Platinum Atoms into Mesoporous Carbon Matrix for Hydrogen Evolution Reaction. Sci. Adv. 2018, 4, eaao6657.

(22). Gong M; Wang DY; Chen CC; Hwang BJ; Dai H. A Mini Review on Nickel-Based Electrocatalysts for Alkaline Hydrogen Evolution Reaction. Nano Res. 2016, 9, 28–46.

(23). Zhang X; Liang Y. Nickel Hydr(oxy)oxide Nanoparticles on Metallic MoS2 Nanosheets: A Synergistic Electrocatalyst for Hydrogen Evolution Reaction. Adv. Sci. 2018, 5, 1700644.

(24). Markovic NM; Sarraf ST; Gasteiger HA; Ross PN Jr. Hydrogen Electrochemistry on Platinum Low-Index Single-Crystal Surfaces in Alkaline Solution. J. Chem. Soc., Faraday Trans. 1996, 92, 3719–3725.

(25). Sheng W; Gasteiger HA; Shao-Horn Y. Hydrogen Oxidation and Evolution Reaction Kinetics on Platinum: Acid vs Alkaline Electrolytes. J. Electrochem. Soc. 2010, 157, B1529–B1536.

(26). Strmcnik D; Lopes PP; Genorio B; Stamenkovic VR; Markovic NM. Design Principles for Hydrogen Evolution Reaction Catalyst Materials. Nano Energy 2016, 29, 29–36.

(27). Subbaraman R; Tripkovic D; Strmcnik D; Chang KC; Uchimura M; Paulikas AP; Stamenkovic V; Markovic NM. Enhancing Hydrogen Evolution Activity in Water Splitting by Tailoring Li+-Ni(OH)2-Pt Interfaces. Science 2011, 334, 1256–1260. [PubMed: 22144621]

(28). Subbaraman R; Tripkovic D; Chang KC; Strmcnik D; Paulikas AP; Hirunsit P; Chan M; Greeley J; Stamenkovic V; Markovic NM. Trends in Activity for the Water Electrolyser Reactions on 3d M(Ni,Co,Fe,Mn) Hydr(oxy)oxide Catalysts. Nat. Mater. 2012, 11, 550–557. [PubMed: 22561903]

(29). Strmcnik D; Uchimura M; Wang C; Subbaraman R; Danilovic N; van der Vliet D; Paulikas AP; Stamenkovic V; Markovic NM. Improving the Hydrogen Oxidation Reaction Rate by Promotion of Hydroxyl Adsorption. Nat. Chem. 2013, 5, 300–306. [PubMed: 23511418]

(30). Yin H; Zhao S; Zhao K; Muqsit A; Tang H; Chang L; Zhao H; Gao Y; Tang Z. Ultrathin Platinum Nanowires Grown on Single-Layered Nickel Hydroxide with High Hydrogen Evolution Activity. Nat. Commun. 2015, 6, 6430. [PubMed: 25728293]

(31). Stamenkovic V; Strmcnik D; Lopes PP; Markovic NM. Energy and Fuels from Electrochemical Interfaces. Nat. Mater. 2017, 16, 57–69.

(32). Wang L; Lin C; Huang D; Chen J; Jiang L; Wang M; Chi L; Shi L; Jin J. Optimizing the Volmer Step by Single-Layer Nickel Hydroxide Nanosheets in Hydrogen Evolution Reaction of Platinum. ACS Catal. 2015, 5, 3801–3806.

(33). Xing Z; Han C; Wang D; Li Q; Yang X. Ultrafine Pt Nanoparticle-Decorated Co(OH)2 Nanosheet Arrays with Enhanced Catalytic Activity toward Hydrogen Evolution. ACS Catal. 2017, 7, 7131–7135.

(34). Zhao Z; Liu H; Gao W; Xue W; Liu Z; Huang J; Pan X; Huang Y. Surface-Engineered PtNi-O Nanostructure with Record-High Performance for Electrocatalytic Hydrogen Evolution Reaction. J. Am. Chem. Soc. 2018, 140, 9046–9050. [PubMed: 29983055]

(35). Wang L; Zhu Y; Zeng Z; Lin C; Giroux M; Jiang L; Han Y; Greeley J; Wang C; Jin J. Platinum-Nickel Hydroxide Nanocomposites for Electrocatalytic Reduction of Water. Nano Energy 2017, 31, 456–461.

(36). Thiel PA; Madey TE. The Interaction of Water with Solid Surfaces: Fundamental Aspects. Surf. Sci. Rep. 1987, 7, 211–385.

(37). Henderson MA. The Interaction of Water with Solid Surfaces: Fundamental Aspects Revisited. Surf. Sci. Rep. 2002, 46, 1–138.

(38). Durst J; Siebel A; Simon C; Hasche F; Herranz J; Gasteiger HA. New Insights into the Electrochemical Hydrogen Oxidation and Evolution Reaction Mechanism. Energy Environ. Sci. 2014, 7, 2255–2260.

(39). Li H; Tsai C; Koh AL; Cai L; Contryman AW; Fragapane AH; Zhao J; Han HS; Manoharan HC; Abild-Pedersen F; Nørskov JK; Zheng X. Activating and Optimizing MoS2 Basal Planes for Hydrogen Evolution Through the Formation of Strained Sulphur Vacancies. Nat. Mater. 2016, 15, 48–53. [PubMed: 26552057]

(40). Zhang J; Wang T; Liu P; Liu S; Dong R; Zhuang X; Chen M; Feng X. Engineering Water Dissociation Sites in MoS2 Nanosheets for Accelerated Electrocatalytic Hydrogen Production. Energy Environ. Sci. 2016, 9, 2789–2793.

(41). Melendres CA; Xu S. In Situ Laser Raman Spectroscopic Study of Anodic Corrosion Films on Nickel and Cobalt. J. Electrochem. Soc. 1984, 131, 2239–2243.

(42). Dharmaraj N; Prabu P; Nagarajan S; Kim CH; Park JH; Kim HY. Synthesis of Nickel Oxide Nanoparticles Using Nickel Acetate and Poly(vinyl acetate) Precursor. Mater. Sci. Eng., B 2006, 128, 111–114.

(43). Watts JF; Wolstenholme J. An Introduction to Surface Analysis by XPS and AES; Wiley: Chichester, U.K., 2003.

(44). Jiao L; Regalbuto JR. The Synthesis of Highly Dispersed Noble and Base Metals on Silica via Strong Electrostatic Adsorption: I. Amorphous Silica. J. Catal. 2008, 260, 329–341.

(45). Wong A; Lin Q; Griffin S; Nicholls A; Regalbute JR. Synthesis of Ultrasmall, Homogeneously Alloyed, Bimetallic Nanoparticles on Silica Supports. Science 2017, 358, 1427–1430. [PubMed: 29170281]

(46). Shi Y; Zhang B. Recent Advances in Transition Metal Phosphide Nanomaterials: Synthesis and Applications in Hydrogen Evolution Reaction. Chem. Soc. Rev. 2016, 45, 1529–1541. [PubMed: 26806563]

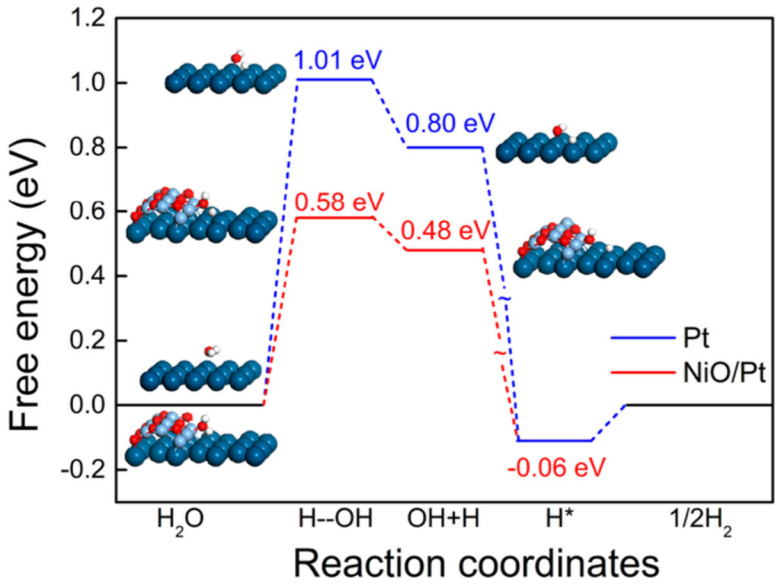

Figure 1.

Calculated free energy diagram for H_2O dissociation and H_2 desorption on the Pt surface (blue) and NiO/Pt interface (red). Insets show the optimized structures at different reaction stages. The large dark blue, small light blue, red, and white balls represent Pt, Ni, O, and H atoms, respectively.

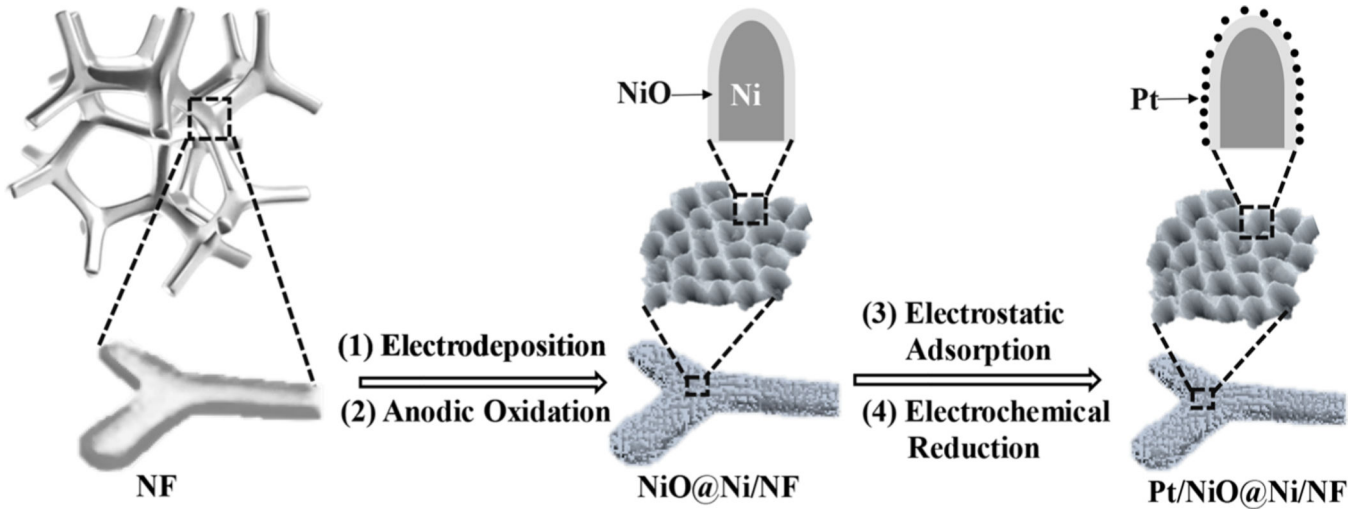

Figure 2.
Schematic illustration for the preparation process of Pt/NiO@Ni/NF catalyst with a honeycomb-like nanostructure.

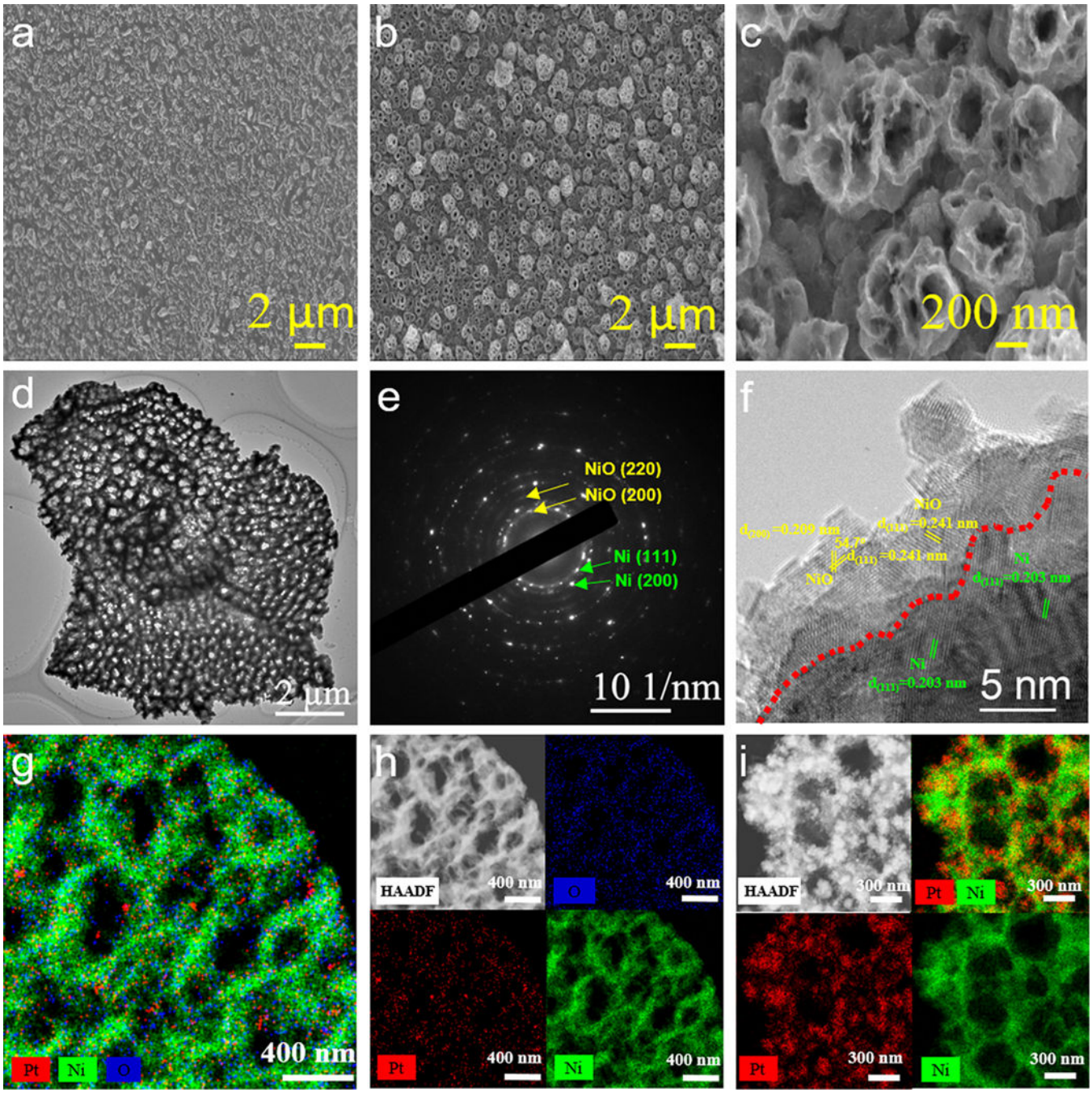

Figure 3.

FE-SEM images of Ni/Cu/NF (a) and NiO@Ni/NF at different resolutions (b, c). TEM image (d), SAED pattern (e), and HRTEM (f) of Pt/NiO@Ni/NF. HAADF-STEM images and the corresponding STEM-EDX elemental mappings of Pt/NiO@Ni/NF (g, h) and Pt@Ni/NF(i).

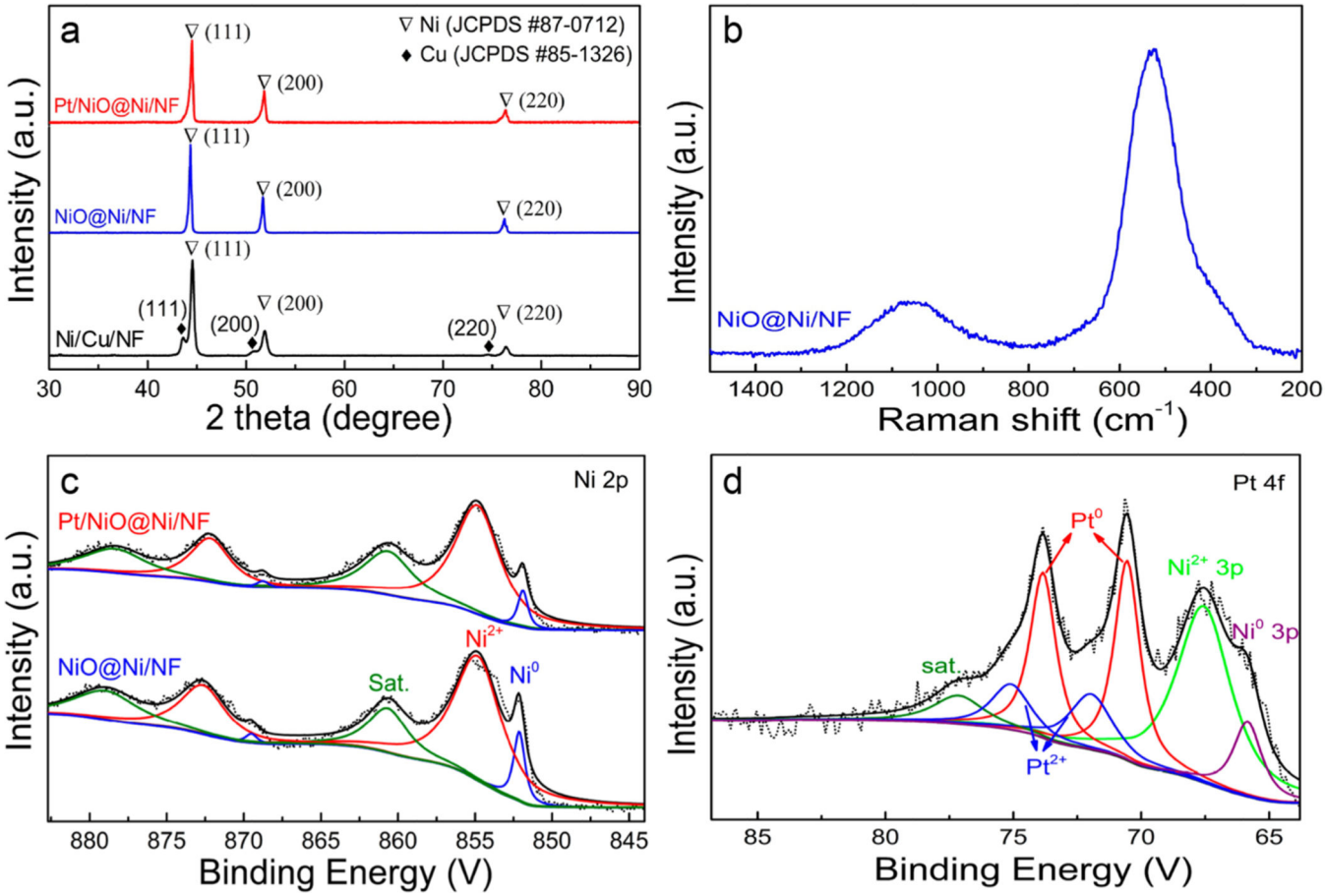

Figure 4.

(a) XRD patterns of Pt/NiO@Ni/NF, NiO@Ni/NF, and Ni/Cu/NF. (b) Raman spectrum of NiO@Ni/NF. (c) Ni 2p XPS spectra of Pt/NiO@Ni/NF and NiO@Ni/NF. (d) XPS spectrum of Pt/NiO@Ni/NF in the Pt 4f region.

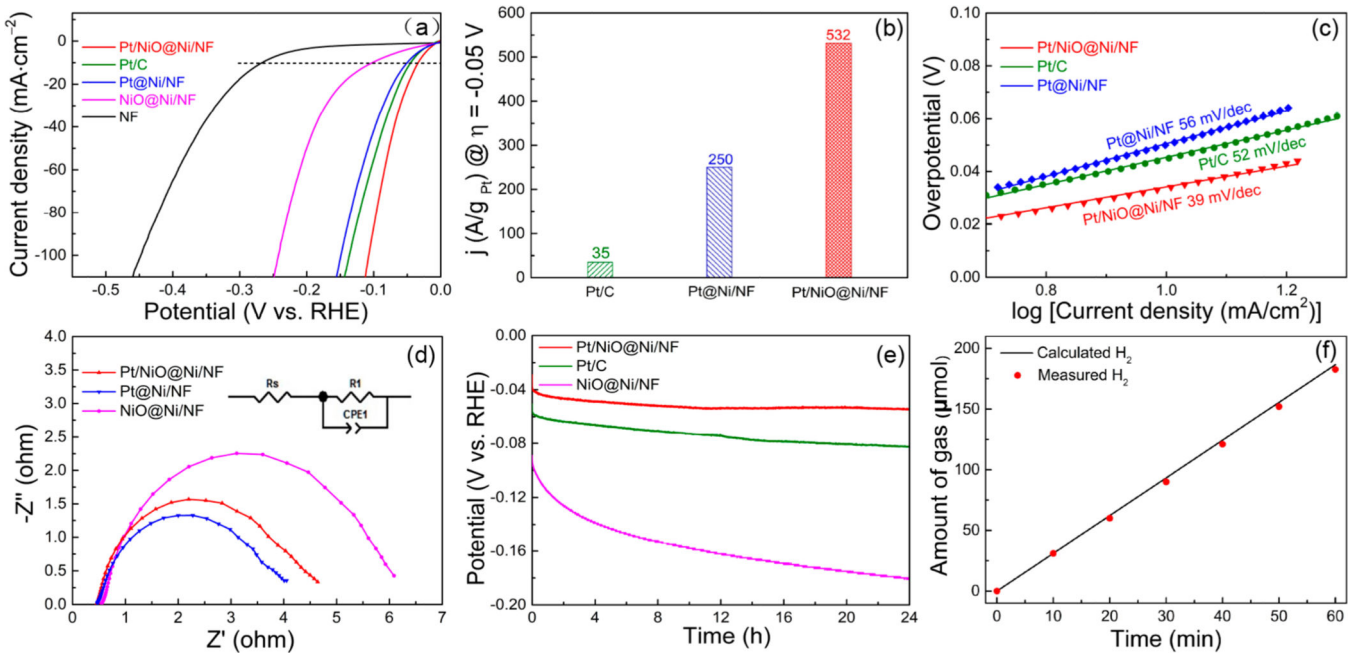

Figure 5.

(a) HER polarization curves of various electrocatalysts. (b) HER mass activities of Pt/C, Pt@Ni/NF, and Pt/NiO@Ni/NF. (c) Corresponding Tafel plots for the various eletrocatalysts. (d) EIS Nyquist plots for Pt/NiO@Ni/NF, Pt@Ni/NF, and NiO@Ni/NF. (e) Chronopotentiometric curve of Pt/NiO@Ni/NF catalyst at 10 mA cm^{-2}. (f) Experimentally measured H_2 production versus theoretically calculated quantities under a constant current density of 10 mA cm^{-2}. Conditions: Pt loading 0.092 mg cm^{-2} (Pt/NiO@Ni/NF), 0.286 mg cm^{-2} (Pt/C), 0.113 mg cm^{-2} (Pt@Ni/NF); NiO@Ni loading ~2.0 mg cm^{-2}; electrolyte 1 M KOH solution; sweep rate 2 mV s^{-1}.